Effects of vertical differencing in a minimal hurricane model

By Hongyan Zhu* and Roger K. Smith

Meteorological Institute, University of Munich, Germany

July 10, 2002

Abstract

The minimal three-layer hurricane model developed by the authors is reformulated with a Charney-Phillips grid (CP-grid) in the vertical instead of the Lorenz grid (L-grid) that was used in the original model. It has been shown by others that the popular L-grid supports a computational mode in the temperature field that can lead to inaccuracies, especially when moist processes are involved. Here we compare calculations of the hurricane model using the L-grid and CP-grid. We present evidence that the computational mode is excited in the L-grid model during the period of rapid vortex intensification, which begins when grid-scale latent heat release occurs in the core region. Thus it would appear that the solution in the mature stage of evolution is contaminated by this mode. We show also that the vortex asymmetries that develop during the mature stage are sensitive to the choice of vertical grid and argue that those that occur in the CP-grid formulation are more realistic. It is possible that the computational mode is a spurious feature of many earlier studies of asymmetries in hurricane models in which moist processes are represented.

1. Introduction

An important step in understanding any meteorological phenomenon is to isolate those processes that are crucial from those that are of secondary importance. With this idea in mind, Charney (1947) and Eady (1949) developed models that are widely regarded as prototype problems for understanding extra-tropical cyclogenesis. Even though these models differ in some important details, they both capture many of the observed features of the structure and energetics of extra-tropical cyclones. In the same spirit one might enquire: what are the prototype problems for understanding tropical cyclone intensification? Possible contenders amongst the early models must surely include the three-layer axisymmetric model of Ooyama (1969) and the three-layer, three-dimensional models of Anthes *et al.* (1971) and Anthes (1972), while the steady axisymmetric analytic model of Emanuel (1988) might be considered to be a prototype model for the mature hurricane. More recent contenders for the intensification problem are the axisymmetric models of Emanuel (1989, 1995) and Nguyen *et al.* (2002), and the minimal three-dimensional model of Zhu *et al.* (2001; henceforth referred to as ZSU). The Nguyen *et al.* model is an axisymmetric version of the ZSU model.

Compared with extra-tropical cyclones, the development of a prototype model for tropical cyclones is complicated by the central importance of deep cumulus convection for the dynamics. Ooyama's model is based on three layers of homogeneous fluid with heating by deep cumulus convection represented by a mass transfer between layers. The amount of mass transferred is based on a simple steady cloud model that conserves mass and moist static energy and which would detrain at neutral buoyancy in upper layer. In Emanuel's formulations, deep cumulus convection is assumed to bring the atmosphere above the boundary layer to a state in which the saturation moist entropy along an angular momentum surface is equal to the moist entropy at the top of the subcloud layer. Thus the

* Corresponding author: Ms. Hongyan Zhu, Meteorological Institute, University of Munich, Theresienstr. 37, 80333 Munich, Germany. Email: hongyan@meteo.physik.uni-muenchen.de

model includes an entropy equation, but water vapour is not carried as a separate variable so that the model cannot predict, for example, the amount of precipitation. In contrast, the Anthes (1972) and ZSU models include a more complete representation of moist processes with both a moisture and thermodynamic equation. ZSU's model has the option to include one of three different parameterizations of deep convection, or to dispense with any such parameterization, allowing for a crude representation of explicit moist processes only.

As with the Charney and Eady problems, all the foregoing hurricane models have their limitations and it would be hard to support a claim that any one is *the* prototype model for a hurricane. Nevertheless, all may be useful for *understanding* tropical cyclone intensification.

A particular limitation of all the simple models is their vertical resolution. For the three-dimensional problem it would seem that a minimum of three vertical layers is required: a shallow boundary layer to allow for the frictionally-induced inflow of moist air; a lower tropospheric layer to allow for inflow above the friction layer; and an upper-tropospheric layer to allow for outflow. In his axisymmetric models, Emanuel elegantly avoids the need for a separate outflow layer by using potential radius* as the radial coordinate, but this is not practical for three-dimensional models.

The limited vertical resolution is an acute problem when moisture is included explicitly in the formulation, as in the Anthes (1972) and ZSU models. There are several reasons for this. First, one cannot accurately represent slantwise moist ascent above the boundary layer with only two layers. Secondly, the specific humidity of moisture is a strongly decreasing function of altitude and is also not accurately represented with three layers. Another potential problem, the subject of the present paper, is the way in which the vertical grid is staggered. The ZSU model uses the staggered grid devised by Lorenz (1960), the so-called L-grid, which is widely used in general circulation and numerical weather prediction models, while the Anthes *et al.* (1971) and Anthes (1972) models use a different configuration (see below). The L-grid has certain desirable attributes: for example, it enables the total energy, the mean potential temperature, and the variance of the potential temperature to be conserved under adiabatic and frictionless processes (Arakawa (1972); Arakawa and Lamb, 1977; Arakawa and Suarez, 1983). However, it has been shown to lead to a computational mode in the vertical distribution of potential temperature (Tokioka, 1978; Arakawa and Moorthi, 1988; Cullen *et al.*, 1997; Hollingsworth, 1995; Arakawa and Konor, 1996; henceforth referred to as AK). The same applies to the grid used by Anthes *et al.* (1971) and Anthes (1972), which appears to have been widely used also (subsequently we refer to this grid as the A-grid). AK cautioned that the existence of the computational mode may be serious, especially in the models that include moist processes, since the computational mode can spuriously interact with the physical mode through inherently nonlinear condensation and associated processes. Both they and Hollingsworth (1995) showed that the problem could be resolved by using the staggered grid proposed by Charney and Phillips (1953), which they call the CP-grid.

In the belief that simple models are of central importance to a basic understanding of complex phenomena, and because of the fact that moist processes are of central important for hurricane intensification, we are led here to compare calculations of vortex evolution and vortex structure in the minimal hurricane model of ZSU using the CP-grid and L-grid. We begin in section 2 with a brief review of the three types of grid, describing the precise problems with the L-grid and A-grid. The model equations are summarized in section 3 and the configuration of the CP-grid model is described in sections 4. The formulation of

* The potential radius is the radius to which an air parcel must be moved (conserving its absolute angular momentum) in order to change its tangential velocity component to zero. It is proportional to the square root of the absolute angular momentum per unit mass about the vortex centre.

physical processes and other aspects of the CP-grid model are described in section 5 and comparisons of simulations with the L-grid and CP-grid are presented in section 6. The conclusions are given in section 7.

2. The L-grid, A-grid and CP-grid

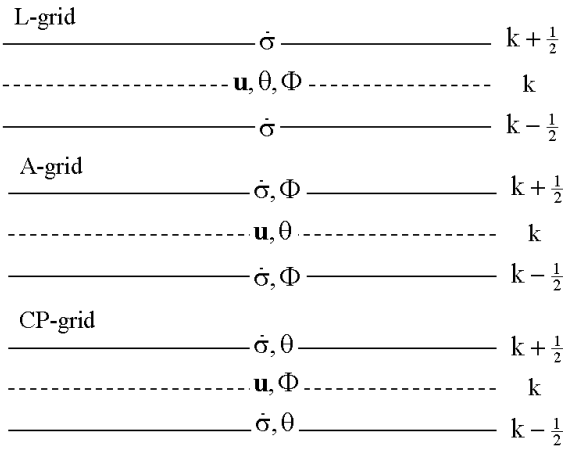

Figure 1. Configuration of σ-levels in the L-grid, A-grid and CP-grid models.

In the L-grid, the (potential) temperature, θ, horizontal velocity, $\mathbf{u}$, and geopotential height, Φ, are stored at the middle of layers, while the vertical velocity is defined at the interfaces between these layers (Fig. 1). AK show that the computational mode arises because of the extra freedom available in the temperature field and typically appears as an oscillation of θ that changes sign from one level to the next. The existence of this oscillation is caused by the fact that, with centered or approximately centred finite differencing, the thickness between two adjacent layers, $\Phi_k - \Phi_{k-1}$ depends on an average of θ between the two layers, i.e. $\theta_{k-1/2} = 0.5(\theta_k + \theta_{k-1})$. It is possible to have a zero vertical distribution of perturbation geopotential ϕ' for a nonzero vertical distribution of perturbation potential temperature θ'. This solution, with an alternating or zigzag temperature perturbation between layers, is uncoupled from the dynamical fields of the discrete system, although it may couple with moist processes by its effect on the saturation vapour pressure. AK pointed out that the existence of a computational mode is a property of any Lorenz-type grid in which the horizontal momentum and potential temperature are carried at the same levels.

Arakawa and Moorthi (1988) showed that use of the L-grid can reduce also the effective static stability and falsely satisfy the necessary condition for baroclinic instability near the lower and upper boundaries.

In the A-grid, Φ is defined at interface levels while the horizontal velocities and potential temperature are stored at the middle of layers. Tokioka (1978) advocated the use of this grid, thinking that the computational mode would be eliminated because the discrete hydrostatic equation does not involve average of potential temperature. However, Arakawa and Moorthi (1988) showed that this is not the case. They noted that for the pressure gradient term in the middle of layers, one still needs to obtain the geopotential height by averaging $\Phi_{k-1/2}$ and $\Phi_{k+1/2}$. The difference $\Phi_k - \Phi_{k-1}$ again depends on an average of

θ_k and θ_{k-1} and the computational mode can still appear. Thus the existence of a computational mode is a feature of any vertical grid in which $\mathbf{u}$ and θ are carried at the same levels, rather than a particular vertical-difference scheme.

AK designed a sigma-coordinate version of the vertical grid used by Charney and Phillips (1953), the structure of which is shown in the lower panel of Fig 2. In the CP-grid, temperature or potential temperature are carried at the interface levels with the vertical $\sigma-$velocity, $\dot{\sigma}$, while the horizontal velocity and the geopotential are calculated in the middle of layers as in the L-grid. AK showed that with this configuration the computational mode does not exist because heat can be transferred by the mass flux at the same level. Also the thickness between two adjacent model layers depends solely upon the potential temperature in between, thus precluding a zigzag temperature pattern in vertical. Arakawa and Moorthi (1988) found that with the CP grid, one can easily maintain important dynamical constraints on quasi-geostrophic flow, such as the conservation of quasi-geostrophic potential vorticity through horizontal advection and the resulting integral constraints. In contrast it is not even straightforward to define quasi-geostrophic potential vorticity, with the L-grid.

3. Governing Equations in the CP-grid model

The basic equations in the CP-grid are similar to those in ZSU. The ZSU model is based on the three-dimensional hydrostatic primitive equations in sigma-coordinates (x, y, σ) on an f-plane or β-plane, where x and y are in the zonal and meridional directions, respectively, and

$$\sigma = \frac{p - p_{top}}{p_s - p_{top}} = \frac{p - p_{top}}{p^*} \tag{1}$$

$p^* = p_s - p_{top}$, p_s and p_{top} are the surface and top pressures and p_{top} is a constant, taken here to be 100 mb. Then the upper and lower boundary conditions require that $\dot{\sigma} = 0$ at $\sigma = 0$ and $\sigma = 1$, where $\dot{\sigma} = D\sigma/Dt$ and D/Dt is the material derivative. The zonal and meridional momentum equations and the hydrostatic equation are:

$$\frac{\partial u}{\partial t} = -\left(u\frac{\partial u}{\partial x} + v\frac{\partial u}{\partial y}\right) - \dot{\sigma}\frac{\partial u}{\partial \sigma} + fv - \frac{RT\sigma}{p}\frac{\partial p^*}{\partial x} - \frac{\partial \Phi}{\partial x} + F_u \tag{2}$$

$$\frac{\partial v}{\partial t} = -\left(u\frac{\partial v}{\partial x} + v\frac{\partial v}{\partial y}\right) - \dot{\sigma}\frac{\partial v}{\partial \sigma} - fu - \frac{RT\sigma}{p}\frac{\partial p^*}{\partial y} - \frac{\partial \Phi}{\partial y} + F_v \tag{3}$$

$$\frac{\partial \Phi}{\partial \sigma} = -\frac{RTp^*}{p} \tag{4}$$

where u and v are the velocity components in the $x-$ and $y-$directions, $f = f_o + \beta y$ is the Coriolis parameter, f_o and $\beta = df/dy$ are constants, R is the specific gas constant for dry air, $\kappa = R/c_p$, c_p is the specific heat of dry air, θ is the potential temperature, Φ is the geopotential, and F_u and F_v represent the frictional drag in the $x-$ and $y-$directions, respectively. In this model, the calculations are carried out on an f-plane at 20°N whereupon β is set to zero. The surface pressure tendency equation, derived from the continuity equation and boundary conditions is

$$\frac{\partial p^*}{\partial t} = -\int_0^1 \left(\frac{\partial (p^* u)}{\partial x} + \frac{\partial (p^* v)}{\partial y} \right) d\sigma \tag{5}$$

and $\dot{\sigma}$ is given by

$$\dot{\sigma} = -\frac{1}{p^*} \int_0^\sigma \left(\frac{\partial (p^* u)}{\partial x} + \frac{\partial (p^* v)}{\partial y} \right) d\sigma + \frac{\sigma}{p^*} \int_0^1 \left(\frac{\partial (p^* u)}{\partial x} + \frac{\partial (p^* v)}{\partial y} \right) d\sigma \tag{6}$$

The thermodynamic and moisture equations are

$$c_p \frac{\partial T}{\partial t} = -c_p \left(u \frac{\partial T}{\partial x} + v \frac{\partial T}{\partial y} \right) - c_p \dot{\sigma} \frac{\partial T}{\partial \sigma} + \alpha \omega + Q_\theta \tag{7}$$

and

$$\frac{\partial q}{\partial t} = -\left(u \frac{\partial q}{\partial x} + v \frac{\partial q}{\partial y} \right) - \dot{\sigma} \frac{\partial q}{\partial \sigma} + Q_q \tag{8}$$

where α is the specific volume, q is the specific humidity, ω is the vertical p-velocity, Q_θ is the diabatic heat source and Q_q is the moisture source. The temperature T is related to θ by the formula

$$T = \left(\frac{p}{p_o} \right)^\kappa \theta = \frac{(p^* \sigma + p_{top})^\kappa}{p_o^\kappa} \theta \tag{9}$$

where $p_o = 1000$ mb.

4. The Vertical differencing in the CP-grid model

The vertically discrete equations are designed to satisfy the four constraints advocated by Arakawa and Lamb (1977), namely:

- the vertically-integrated pressure gradient force generates no circulation along a contour of any surface topography;
- the energy conversion terms in the thermodynamic and kinetic energy equations have the same form with opposite signs so that the total energy is conserved under adiabatic frictionless processes;
- the global mass integral of the potential temperature is conserved under adiabatic processes;
- the global mass integral of a function of the potential temperature, such as the square of logarithm of the potential temperature, is conserved also under adiabatic processes.

As in ZSU, the model is divided vertically into three unequally deep layers with σ-depths of $\frac{3}{9}$, $\frac{5}{9}$, $\frac{1}{9}$, respectively from the top layer to the lowest layer (see Fig. 2). In the L-grid model, all the dependent variables such as horizontal velocity, potential temperature, specific humidity and geopotential, are defined in the middle of each layer (full levels in the Fig.1), and $\dot{\sigma}$ is staggered. In the CP-grid model, the horizontal velocity, geopotential are calculated at levels 1, 2, and 3, and the potential temperature, specific humidity, and vertical velocity, $\dot{\sigma}$, are stored at levels $\frac{1}{2}, 1\frac{1}{2}, 2\frac{1}{2}$ and $3\frac{1}{2}$. The equations are expressed in finite-difference form in both the horizontal and vertical and integrated forward in time using the Adams-Bashforth third-order method. The discrete equations are based on the scheme formulated by AK and are detailed in the Appendix.

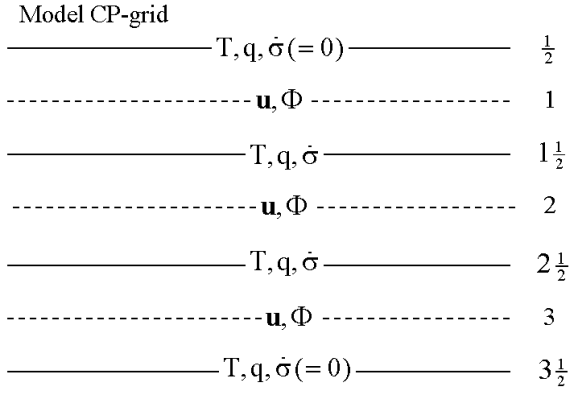

Figure 2. Configuration of σ-levels in the CP-grid model showing locations where the dependent variables are stored. The horizontal velocity, geopotential are calculated at levels 1, 2, and 3, and potential temperature, specific humidity, vertical velocity, $\dot{\sigma}$, are stored at levels $\frac{1}{2}, 1\frac{1}{2}, 2\frac{1}{2}$ and $3\frac{1}{2}$. In contrast to Fig. 1 we use convention in the model that the index k increases downwards.

5. Physical processes in the CP-grid and L-grid models

(*a*) *Explicit moist processes*

Explicit condensation is treated in a similar way to ZSU. If at any time the air becomes supersaturated at a grid point, the specific humidity is set equal to the saturation specific humidity and the excess water vapour is condensed to liquid water. This water is assumed to precipitate out while the latent heat released is added to the air. The latent heat raises the air temperature and thereby the saturation specific humidity, requiring a further adjustment of the amount of condensed water, and so on. Four iterations are sufficient to determine the final amount of water condensed and latent heat released.

(*b*) *Parameterized deep convection*

The reformulation of the mass flux parameterization scheme for deep convection from the L-grid to the CP-grid is not straightforward and will be discussed elsewhere. Calculations using the L-grid model have shown that even when a convection scheme is included, the problems that arise with this grid are associated with the explicit release of latent heat. Therefore we do not include a sub-grid-scale representation of deep convection in the present calculations.

(*c*) *Radiative cooling*

A Newtonian cooling term, $-(\theta - \theta_{ref})/\tau_R$, is added to the right-hand-side of the thermodynamic equation to crudely represent the effect of radiative cooling. In this expression θ_{ref} is the initial potential temperature profile of the basic state and τ_R is a radiative time scale. Here τ_R is set to be 10 days, based on the radiation calculations in Mapes and Zuidema (1996: see Fig. 15b). This is in contrast to ZSU, who like other authors (e.g Rotunno and Emanuel, 1987; Emanuel, 1989, 1995) set τ_R to be 12 h. The implications of this change are discussed in section 6c.

(*d*) *Surface turbulent fluxes*

Following Anthes (1972), the surface drag, in vector notation, is written for the σ-system as

$$p^*(F_u, F_v) = -g\frac{\partial \tau_{\mathbf{z}}}{\partial \sigma} \tag{10}$$

where g is the acceleration due to gravity and $\tau_{\mathbf{z}}$ is the vector Reynolds stress. The quadratic stress law with the surface wind speed approximated by the speed at level-3 is employed for the stress at $\sigma = 1$. Therefore the surface drag is:

$$p^*(F_u, F_v) = \frac{-g\rho^* C_D |\mathbf{v_3}| \mathbf{v_3}}{\delta\sigma_3} \tag{11}$$

where $\mathbf{v_3}$ is the horizontal wind vector at level-3 and $\delta\sigma_3$ is the depth of boundary layer. The drag coefficient, C_D, is defined to be 3×10^{-3} and the surface density, ρ^*, is set to a standard value of 1.10 kg m^{-3}.

For the CP-grid, the sensible and latent heat fluxes at the air-sea interface are given by

$$\begin{aligned} p^* F_q &= \frac{g C_E |\mathbf{v_3}| \rho^* (q^*_{sea} - q_{3\frac{1}{2}})}{0.5\delta\sigma_3}, \\ p^* F_{SH} &= \frac{g c_p C_E |\mathbf{v_3}| \rho^* (T_{sea} - T_{3\frac{1}{2}})}{0.5\delta\sigma_3} \end{aligned} \tag{12}$$

where F_q and F_{SH} are the latent and sensitive heat fluxes added per unit mass and time at level $3\frac{1}{2}$. The exchange coefficient, C_E, is assumed to be the same as C_D. The sea surface temperature is taken to be 28°C. Because $T_{3\frac{1}{2}}$ represents the average temperature between level-3 and level-$3\frac{1}{2}$, the sensible and latent heat fluxes are averaged over half the depth of the boundary layer.

The sensible and latent heat fluxes for the L-grid model at the midlevel of the boundary layer are calculated from the expressions:

$$\begin{aligned} p^* F_q &= \frac{g C_E |\mathbf{v_3}| \rho^* (q^*_{sea} - q_3)}{\delta\sigma_3} \\ p^* F_{SH} &= \frac{g c_p C_E |\mathbf{v_3}| \rho^* (T_{sea} - T_{surface})}{\delta\sigma_3} \end{aligned} \tag{13}$$

As in Anthes (1972)'s formulation, the contributions from F_q and F_{SH} are used to increase the entropy in the boundary layer. It is assumed that the boundary layer is well mixed so that the specific humidity and potential temperature are uniform in the vertical within the boundary layer. Therefore q_3 is used to represent the surface layer specific humidity, and $T_{surface}$ is calculated at a level 3.30 mb above the surface.

(*e*) *Boundary, initial conditions and subgrid-scale diffusion*

The following is a brief summary of model characteristics, details of which can be found in ZSU:

- The calculations are carried out in a zonal channel with rigid walls at $y = \pm Y$ and periodic boundary conditions at $x = \pm X$. It is assumed that there is no motion normal to the meridional boundaries (i. e. $v = 0$ at $y = \pm Y$) and that meridional gradients are zero at these boundaries (i.e. $\partial(u, \theta, q)/\partial y = 0$ at $y = \pm Y$). The computational domain size is 2000 × 2000 km and the grid resolution is 20 km.

- The initial vortex is axisymmetric and barotropic with a maximum tangential wind speed of 15 m s^{-1} at a radius of 120 km.
- The initial mass and geopotential fields are obtained by solving the inverse balance equation.
- The far-field temperature and humidity structure are based on the mean West Indies sounding for the hurricane season (Jordan 1957).
- Horizontal variations of specific humidity in the presence of the initial vortex are neglected.
- The surface pressure in the environment is 1015 mb, and the minimum surface pressure at the vortex centre is initially 1008 mb.
- A fourth-order horizontal diffusion term $D_4 = -k_1 \nabla_h^4 \chi$ is added to all prognostic equations with a diffusion coefficient $k_1 = 0.0008\Delta^4$, where ∇_h is the horizontal Laplacian operator and Δ is the horizontal grid spacing. This subgrid-scale diffusion is used to filter out the energy in high frequency waves. At the boundaries, a second-order diffusion term $D_2 = k_2 \nabla_h^2 \chi$ is applied with $k_2 = 0.0008\Delta^2$.

6. Comparison of results using the CP-grid and L-grid

We compare here the results of two calculations on the f-plane, one using the L-grid and the other using the CP-grid. The vertical differencing in the L-grid model is based on the method proposed by Arakawa and Suarez (1983) and is described by ZSU.

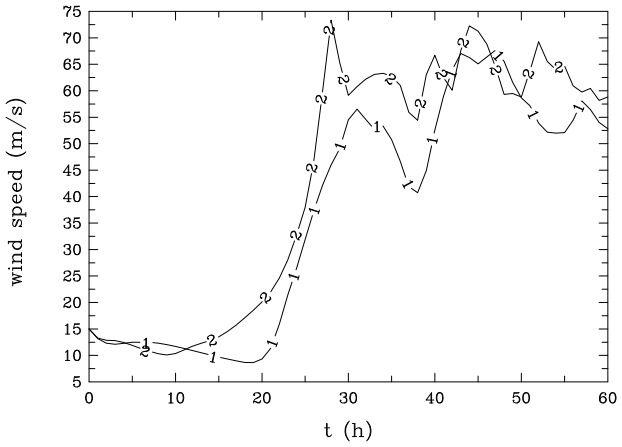

Figure 3. The maximum wind speed in the boundary layer in the L-grid (curve labelled 1) and CP-grid (curve labelled 2) calculations. [Units: m s^{-1}]

Figure 3 compares the maximum wind speed in the boundary layer for the two calculations and would appear to indicate that vortex evolution is quite similar. With the CP-grid, the vortex begins to intensify about 10 h earlier than with the L-grid because saturation occurs earlier in the core region. In the mature stage, the maximum wind speed is about 5 m s^{-1} larger than with the L-grid, but the fluctuations in intensity are larger in the latter case. The differences during the mature stage can be attributed to the difference in the asymmetries that develop in the two calculations (see subsection (b) below). More detailed comparisons of the two calculations are discussed below.

The processes involved in the vortex evolution using the L-grid are discussed at length in ZSU: only the salient features are described here. During the gestation period, which lasts for about 24 h, the vortex slowly decays on account of the frictionally-induced divergence in the lower troposphere (middle layer) and the associated ascent leads to a cooling and moistening of the middle and upper layers in the core region. Eventually, saturation occurs on the grid-scale in the inner core region in the middle and upper layers and the accompanying latent heat release creates positive buoyancy. In turn, the buoyancy leads to convergence in the middle layer, dominating the frictionally-induced divergence in this region (see Smith 2000, section 2). The period of rapid deepening (between 24 h and 30 h) begins with the occurrence of grid-scale saturation. A similar pattern of evolution occurs in the calculations with the CP-grid, but there are notable differences in the temperature fields that develop in the two calculations and in the asymmetries. We examine these differences in the next two subsections.

(*a*) *Temperature field*

Figure 4 compares time-radius plots of the azimuthally-averaged potential temperature deviation at the three model levels at which the temperature is predicted in the two calculations (note that these levels are a little different in the two grids). We consider first the calculation for the L-grid (left panels in Fig. 4). After 30 h, the vortex reaches a mature stage with a warm core in the upper and middle layers indicated by a positive potential temperature deviation. The highest temperature anomaly is about 16^oC at 48 h in the top layer and about 6^oC in the middle layer. After the vortex reaches maturity at about 30 h, the warm anomaly in the top layer extends progressively outwards on account of radial advection in this layer: for example, the 8^oC temperature anomaly contour reaches a radius of 350 km after 60 h. A striking feature of the calculation is that during the same period, a cold anomaly forms in the middle layer in an annular region from 100 km - 300 km with a corresponding warm anomaly in the boundary layer and these spread outwards at about the same rate as the warm anomaly in the upper layer. Note also that the warming in the middle layer in the core region is accompanied by cooling in the boundary layer under the eye region, despite the presence of sensible heat fluxes from the ocean surface (which will be spuriously enhanced by the low temperature anomaly). This zigzag pattern in the potential temperature anomaly during the mature stage is reminiscent of the behaviour of the computational mode in temperature described by AK and Hollingsworth (1995) and it begins to develop when latent heat release occurs. Additional support for the hypothesis that these structures are a manifestation of the computational mode is provided by an examination of the corresponding vertical velocity fields.

The left panels of Fig. 5 show the evolution of the azimuthally-averaged vertical $\sigma-$velocity ($\dot{\sigma}$) at levels $1\frac{1}{2}$ and $2\frac{1}{2}$ for the L-grid calculation. Ascent in the core region (the innermost 100 km) increases rapidly after 24 h, and there is comparatively weak subsidence outside this region and along the axis, the latter indicating the attempt of the model vortex to form an eye-like feature, despite the relatively coarse radial grid-spacing of 20 km. The negative temperature tendency in the middle layer outside the core region is inconsistent with the subsidence that occurs there and is a strong indication that the computational mode is involved.

The temperature fields in the calculation with the CP-grid (right panels of Figs. 4) have a similar structure to those with the L-grid during the gestation period, but, as noted above, grid-scale saturation and vortex intensification occur 10 h earlier in this case. As the vortex starts to rapidly intensify, the warm potential temperature anomaly at all three levels remains mainly within region of radius of 150 km, and does not spread out in the top layer as it does with the L-grid. Moreover, there is no indication of any zigzag pattern in its

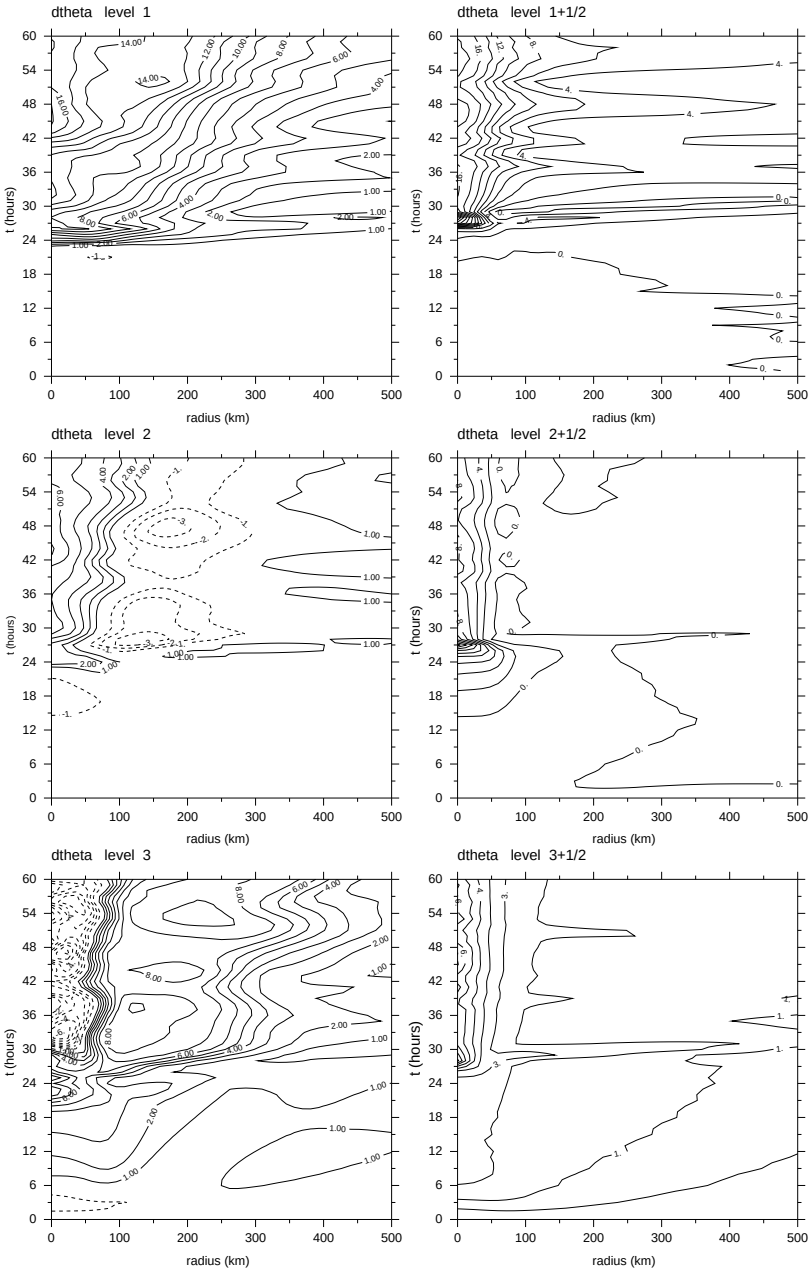

Figure 4. Potential temperature deviation in the top, middle and boundary layer (levels 1, 2 and 3, respectively) in the L-grid calculation (left panels, contour intervals are 1 ^{o}C)) and at levels $1\frac{1}{2}, 2\frac{1}{2}$ and $3\frac{1}{2}$ in the the CP-grid calculation (right panels). [Contour intervals are 2 ^{o}C at levels $1\frac{1}{2}, 2\frac{1}{2}$ and 1 ^{o}C at level $3\frac{1}{2}$)

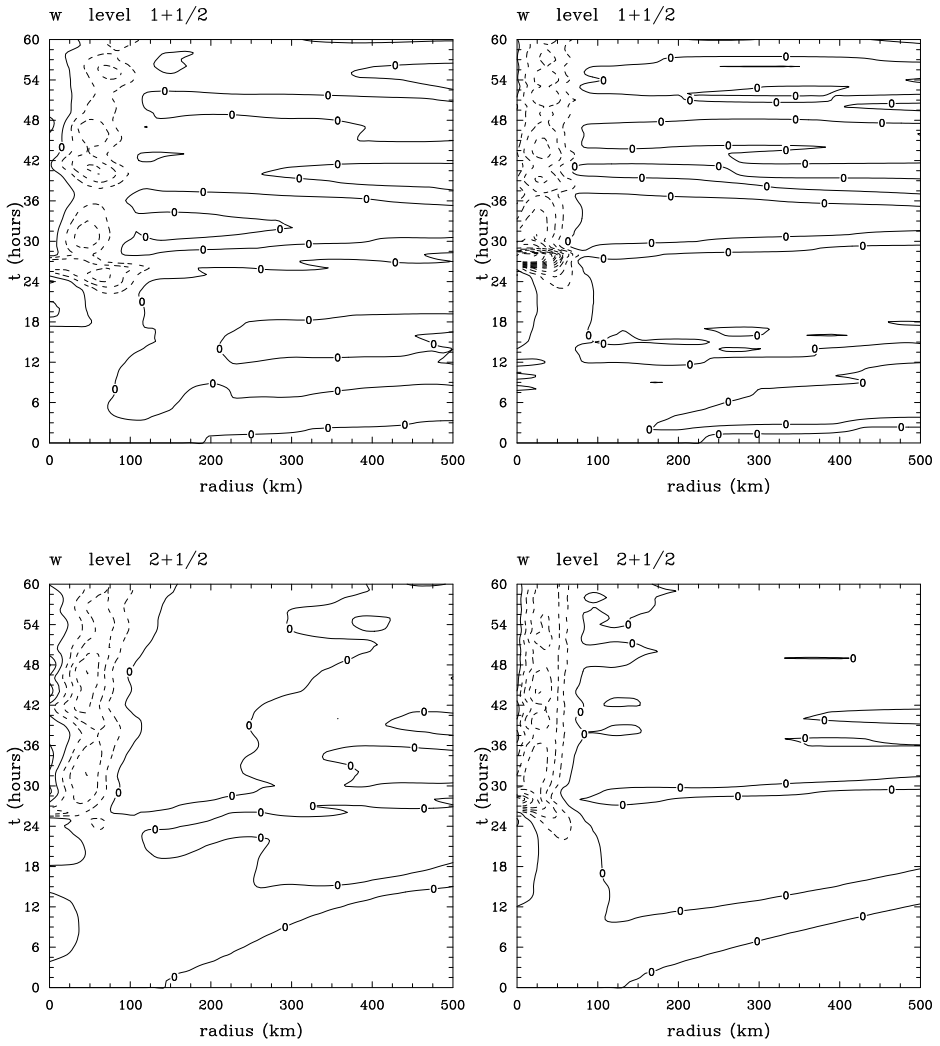

Figure 5. Vertical σ-velocity, $\dot{\sigma}$, at levels $1\frac{1}{2}$ and $2\frac{1}{2}$. Contour interval is 4×10^{-5} s^{-1}. Left panel are for the L-grid calculation, right panel for the CP-grid calculation. The negative values, which indicate ascent, are dashed.

vertical structure. The vertical velocity field in this case is quite similar to that in L-grid (right panels of Fig. 5), but now the temperature field is consistent with the vertical motion. The foregoing results are in agreement with those from comparisons of the two grids in the idealized flows discussed by AK (see Figs. 3 and 4 of their paper) and Hollingsworth (1995, Fig. 4),

Despite the evidence presented for the existence of a computational mode in the temperature field in the calculation with the L-grid, the effect of this mode is small until condensation and heat release occurs in the core region. The same is true also when a convection scheme is included in the calculations (plots not shown). Thus the results pre-

sented here do not detract from the principal results obtained by ZSU and Zhu and Smith (2002), which focus mainly on the earlier periods of evolution. However, they have major implications for using the ZSU model (and its forerunners discussed earlier) for studies of the mature stage of a tropical cyclone.

(*b*) *Development of asymmetries*

ZSU showed that the fluctuations in vortex intensity during the mature stage of development are associated with pronounced asymmetries of the vortex that begin to form when the vortex starts to rapidly intensify. A preliminary study of these asymmetries indicates that their structure depends, *inter alia* on the particular convection scheme chosen for the calculations. We show here that the asymmetries are also strongly influenced by the choice of vertical grid, a finding that is likely to be true of the asymmetries in other calculations, such as those of Anthes (1972) and Kurihara and Tuleya (1974).

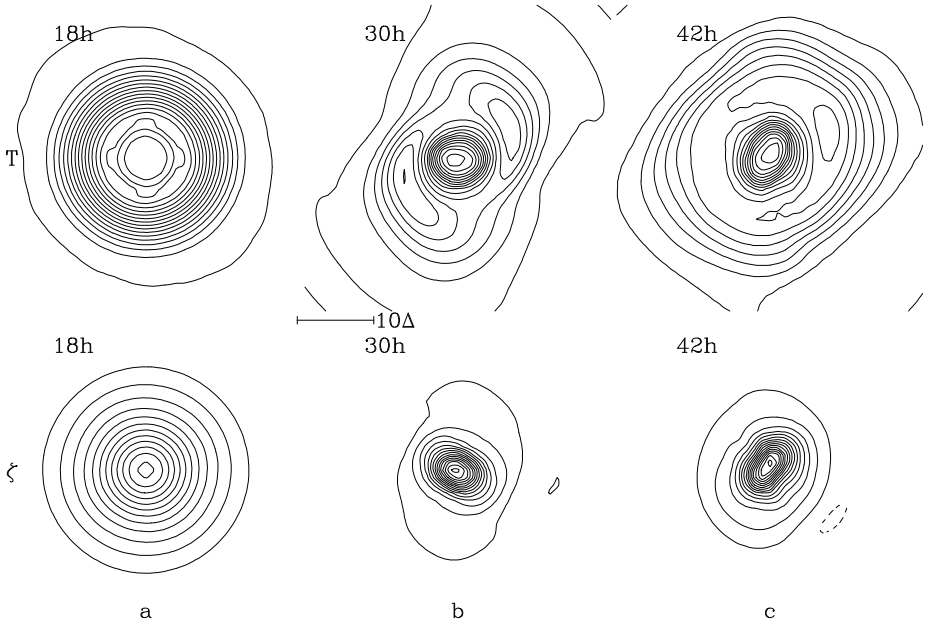

Figure 6. The temperature and vorticity structure in the middle layer at $t = 18$ h, 30 h, and 42 h in the L-Grid calculation. The contour intervals for the temperature field are 5×10^{-2} ^{o}C, 5×10^{-1} ^{o}C, and 2.0×10^{-1} ^{o}C at $t = 18$ h, 30 h, and 42 h respectively. The contour intervals for the vorticity field are 2×10^{-5} s^{-1}, 1×10^{-4} s^{-1}, and 1×10^{-4} s^{-1} at $t = 18$ h, 30 h, and 42 h respectively.

Figures 6 and 7 show the development of the asymmetries in the temperature and vorticity fields at the three chosen times in the middle layer for the calculations with the L-grid and CP-grid. One common feature in both calculations is the azimuthal wavenumber-4 pattern about the vortex centre that begins to emerge prior to the period of rapid intensification. ZSU hypothesize that the emergence of this asymmetry is associated with the representation of an axisymmetric flow on a square grid, a result supported by the calculations of Nguyen *et al.* (2002). At 18 h in Fig. 6a, both the temperature field and vorticity field are quite symmetric about the domain centre, except inside a radius of about 100 km, where a wavenumber-4 pattern is evident. Figure 6b shows that there are wavenumber-2 asymmetries in both temperature and vorticity field at 30 h in this calculation. In the

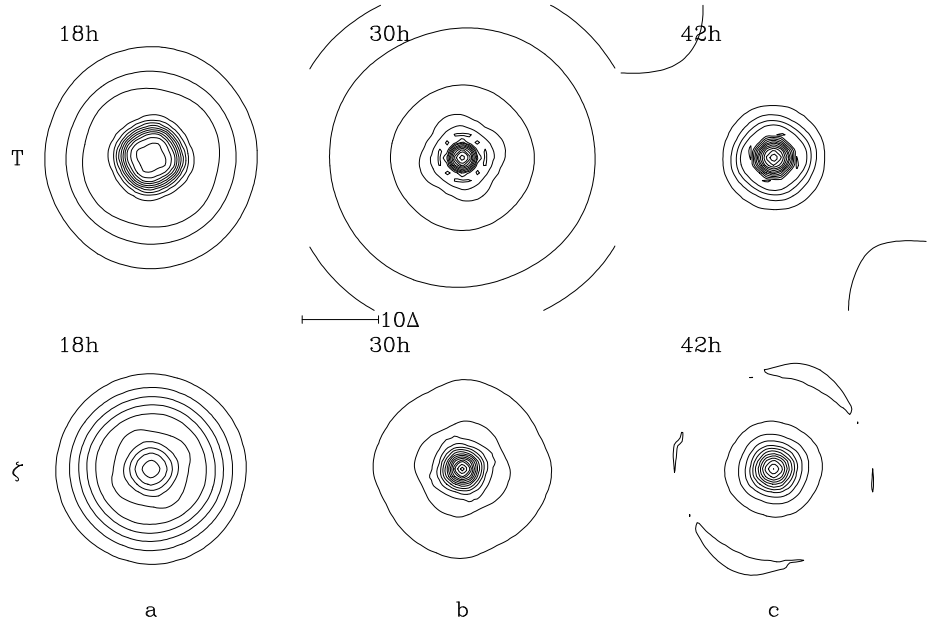

Figure 7. The temperature and vorticity structure at $t = 18$ h, 30 h and 42 h in the calculation with the CP-grid. The contour intervals for the temperature field are 2.0×10^{-1} ^{o}C, 5.0×10^{-1} ^{o}C, and 5.0×10^{-1} ^{o}C at $t = 18$ h, 30 h, and 42 h, respectively. The contour intervals for the vorticity field are 2.5×10^{-5} s^{-1}, 2.5×10^{-4} s^{-1}, and 2.0×10^{-4} s^{-1} at $t = 18$ h, 30 h, and 42 h, respectively.

temperature field, the wavenumber-2 asymmetry appears as two centres of low temperature outside an inner warm core. We noted earlier that a cold temperature anomaly forms in the middle layer outside of the core region when the vortex starts to rapid intensify. Figure 6c shows that the asymmetry at 42 h is similar to that at 30 h, but by this time it has formed a wavenumber-1 component. A linear stability analysis of the initial wind profile by the method of Weber and Smith (1993) shows that it is barotropically unstable to a disturbances of azimuthal wavenumber-2, but the e-folding time scale of this mode is on the order of 66 h, while the wavenumber-2 asymmetry in the L-grid calculation starts at the same time when the vortex core is saturated, which is about 24 h. Therefore it is possible that the zigzag temperature pattern associated with the computational mode in the L-grid has an effect on inducing the wavenumber-2 asymmetry instead of the dynamic instability, and that it contributes to communicating the wavenumber-2 asymmetry downwards to the lower layers. In contrast, with the CP-grid, the vortex is quite symmetric and a wavenumber-4 asymmetry predominates during the gestation and rapid intensification stages. In this calculation, the positive potential temperature anomalies remain essentially in the core region, and the amplitude of the wavenumber-2 component of asymmetry is much less than in the case of the L-grid. So far we do not have an explanation for why there should be such a profound difference between the asymmetries in the calculations with the L-grid and CP-grid, but the mere fact that such a difference exists is significant and suggests caution in the interpretation of the results from the earlier studies discussed below.

Anthes (1972) and Kurihara and Tuleya (1974) studied also the development of asymmetries in calculations for an initially axisymmetric vortex on an f-plane in an environment at rest. Both these studies employed the A-grid described in section 2. As in our L-grid calculation, they found that azimuthal wavenumber-4 is the main feature in the early stage

of development and that wavenumber-2 asymmetries appear with the onset of grid-scale latent heat release. Anthes (1972) found that during the early (symmetric) stage, the variance of any quantity is small and that wavenumber-4 accounts for nearly all the variance. He attributed this asymmetry to artificial aspects of the irregular boundary in his model. At a later stage, with the rapid growth of the variance, wavenumbers-1 and -2 became its dominant contributors. Anthes (1972) showed that the mechanism for the growth of the asymmetries is the barotropic conversion of mean azimuthal kinetic energy to eddy kinetic energy, while Kurihara and Tuleya (1974) found that baroclinic as well as barotropic energy conversions account for the asymmetries in their model. Both papers investigated the spiral rain bands that form in the mature stage of their tropical cyclone simulations. These bands rotate cyclonically about the storm center while propagating outwards and were presumed to be internal gravity waves modified by latent heat release. However all three authors admitted that the mechanism for the spiral bands is unknown, noting that there does seem to be an interesting, although obscure relationship between the bands and the asymmetries. Kurihara and Tuleya (1974) plotted the distribution of temperature field at the mature stage, showing that the front part of the band is relatively warm, while the rear part of the band is cooler. The situation in the upper troposphere is opposite to that at lower levels. Arakawa and Moorthi (1988, p1692) pointed out that the computational mode in temperature is still present with the A-grid, a fact that raises the possibility that the wavenumber-2 and wavenumber-1 asymmetries in Anthes and Kurihara and Tuleya's studies may be associated with the computational mode in temperature also.

(*c*) *Radiative cooling effects*

The excellent discussion of radiative effects in hurricanes by Anthes (1979) indicates that the radial extent of the secondary circulation of a mature hurricane may be expected to be strongly influenced by radiative cooling in the surrounding clear-air environment. In their model, Rotunno and Emanuel (1987) assume a Newtonian relaxation time, $\tau = 12$ h, which yields a cooling rate in the outer regions of approximately 2 K d^{-1}. They argue that this is enough to balance the gentle, but persistent subsidence in the outer regions of the vortex. The same value for τ was used by Emanuel (1989, 1995) and ZSU. Rotunno and Emanuel note, however, that with this value, the cooling rate becomes unrealistically large in the central region where potential temperature becomes significantly larger than the reference value. Both Rotunno and Emanuel (1987) and Emanuel (1989) carried calculations with less radiative cooling and also without it, and found that the temperature anomaly expands to a larger radius than in the corresponding control run.

Some authors would claim that the 12 h time scale for Newtonian cooling is too short: for example the study by Mapes and Zuidema (1996; see Fig. 15b) suggests that it should be about 10 d, which is the value chosen by Arakawa and Moorthi (1988). For this reason we chose $\tau = 10$ d in this paper.

The left panels of Fig. 8 show the potential temperature deviation at the level-1 and -2 in the calculation with the L-grid when τ is set to be 12 h (cf. Fig. 4, two upper left panels). It is clear that the radial spread of the temperature anomaly at the top layer is less than in the case of $\tau = 10$ d . For example, the 8^oC temperature anomaly contour is at about 150 km after 60 h of integration, compared with about 300 km in the calculation with $\tau =$ 10 d. As a result, the cold temperature anomaly within the radius of 100 - 200 km in the middle layer is less than in the case of $\tau = 10$ d. Therefore the strong radiative damping suppresses the computational mode in the L-grid model. It should be noted that Rotunno and Emanuel (1987)'s model uses the L-grid as well and the expansion of the vortex in their calculation without radiation cooling might be associated with the computational mode, even though their model has a higher vertical resolution compared with ours (20

grid distances in the vertical compared with 3). This may explain why it is necessary to have a strong radiative cooling ($\tau = 12$ h) to keep the vortex from expanding.

In contrast, the time-scale for the radiative cooling has less effect on the vortex evolution in CP-grid model. The right panels of Fig. 8 show the potential temperature deviation at the levels $1\frac{1}{2}$ and $2\frac{1}{2}$ in the CP-grid calculation when $\tau = 12$ h. In comparison with the upper two right panels of Fig. 4, the strength of the warm core is reduced by the stronger radiative cooling, but there is no obvious difference in the radial temperature structure.

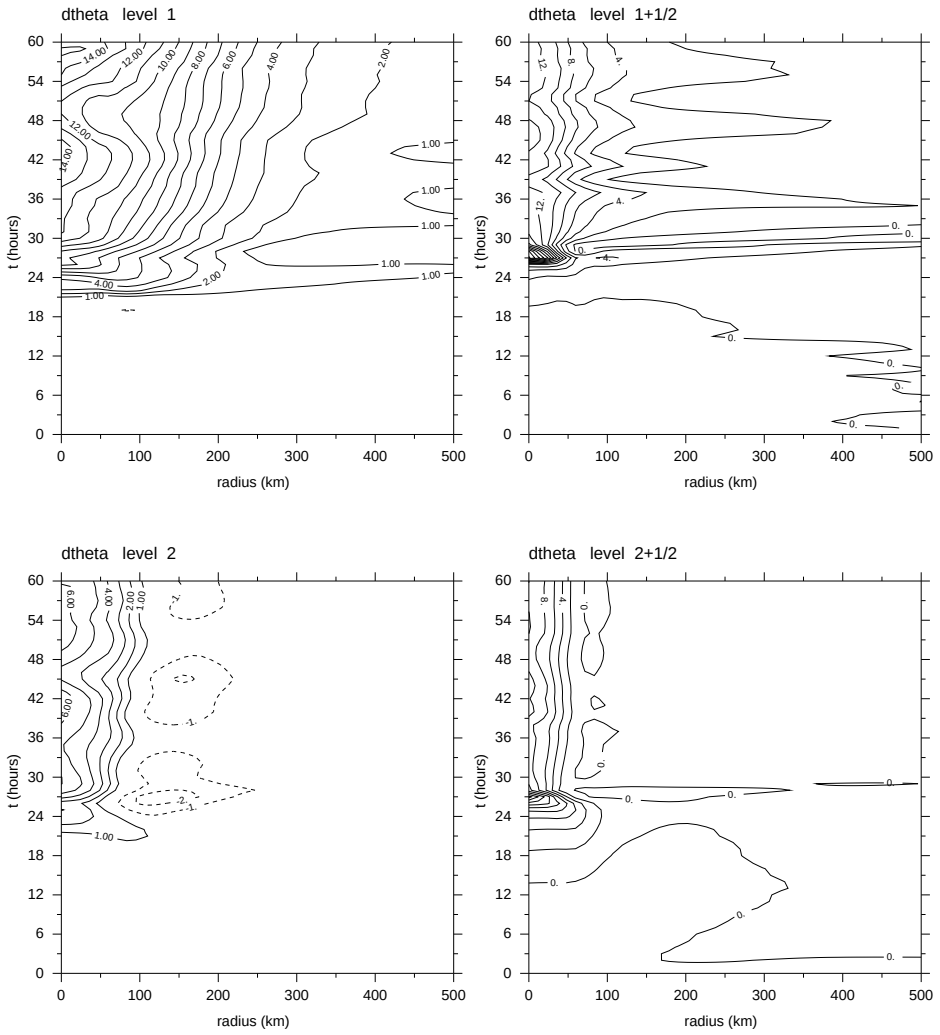

Figure 8. Potential temperature deviation at levels 1 and 2 in the L-Grid calculation (left panel, contour interval 1 ^{o}C.) and at levels $1\frac{1}{2}$ and $2\frac{1}{2}$ in the CP-Grid calculation (right panel, contour interval 2 ^{o}C). The time scale for Newtonian cooling, τ, is 12 h. (Compare with Fig. 4)

7. Conclusions

The minimal hurricane model developed by ZSU has been reformulated on a Charney-Phillips vertically-staggered grid and the results of calculations with a simple explicit representation of moist processes have been compared with those of the original model, which employs the Lorenz-grid. While there is not much difference between the two calculations during the early stages of evolution, the calculation on the L-grid shows evidence of the development of the computational mode in temperature when latent heat release occurs in the inner core of the developing vortex. The existence of this mode raises questions about aspects of the vortex structure during the mature stage of development as well as the structure of the asymmetries that develop during this stage. The same questions could be raised concerning the results of most earlier studies of the evolution of asymmetries in hurricanes, where the models used employ a vertical-staggered grid that also permits a computational mode in temperature.

Use of the CP-grid with the conservative finite-difference scheme worked out by Arakawa and Konor (1996) appears to avoid the problems of the L- and A-grids and the asymmetries that form during the mature stage of development are more consistent with expectations in a flow on an f-plane emerging from axisymmetric initial conditions, assuming that dynamical instabilities are not involved. Weak azimuthal wavenumber-4 asymmetries are present during the gestation period in both models and appear to be related to the representation of a circular flow on a square grid as the initial vortex profile, at least, is *barotropically stable* to this wavenumber. In the L-grid model, an azimuthal wavenumber-2 pattern develops during the period of rapid intensification as the zigzag temperature pattern appears out of the core region and later, the asymmetry acquires wavenumber-1 components as has been seen in some of the earlier calculations. With the CP-grid, the warm core is much more confined in radius and the wavenumbers-1 and -2 components that develop later in the integration are much weaker in amplitude.

Acknowledgements

We are grateful to Brian Mapes for drawing our attention to the potential problems of the computational mode when using the L-grid. We thank Harry Weber also for providing the code to investigate the barotropic stability of our initial vortex profile. This work was supported by the US Office of Naval Research through Grant No. N00014-95-1-0394.

References

Anthes, R. A., J. W. Trout and S. L. Rosenthal 1971 Comparisons of tropical cyclone simulations with and without the assumption of circular symmetry. *Mon. Wea. Rev.*, **99**, 759-766

Anthes, R. A. 1972 Development of asymmetries in a three-dimensional numerical model of a tropical cyclone. *Mon. Wea. Rev.*, **100**, 461-476

Anthes, R. A. 1979 Modelling of tropical cyclones and their environment. *Aust. Meteor. Mag.*, **27**, 213-228

Arakawa, A. 1972 Design of the UCLA general circulation model. Numerical Simulation of Weather and Climate, *Tech. Rep. No.7, Dept. of Meteorology, University of California*, 116 pp

Arakawa, A., and V. Lamb 1977 Computational design of the basic dynamical processes of the UCLA general circulation model. *Methods in Computational Physics*. Vol. **17**, J. Chang, Ed., Academic Press, 173-265

Arakawa, A., and M. J. Suarez	1983	Vertical differencing of the primitive equations in sigma coordinates. *Mon. Wea. Rev.*, **111** 34-45
Arakawa, A., and S. Moorthi	1988	Baroclinic instability in vertically discrete systems. *J. Atmos. Sci.*, **45** 1688-1707
Arakawa, A., and C. S. Konor	1996	Vertical differencing of the primitive equations based on the Charney-Phillips grid in hybrid $\sigma - p$ vertical coordinates. *Mon. Wea. Rev.*, **124** 511-528
Mapes, B. E., and P. Zuidema	1996	Radiative-dynamical consequences of dry tongues in the tropical troposphere. *J. Atmos. Sci.*, **53** 620-638
Charney, J. G.	1947	The dynamics of long waves in a baroclinic westerly current. *J. Meteor.*, **4**, 135-162
Charney, J. G., and N. A. Philips	1953	Numerical integration of the quasi-geostrophic equations for barotropic and simple baroclinic flows. *J.Meteor.*, **10**, 71-99
Cullen, M.J.P., T. Davies, M. H. Mawson, J. A. James, S. C. Coulter and A. Malcolm	1997	An overview of numerical methods for the next generation U. K. NWP and climate model. *Numerical methods in atmospheric and ocean modelling. The Andre J. Robert memorial volume. (Ed. C. A. Lin). Rene Laprise and Harold Ritchie.*, 425-444.
Eady, E. T.	1949	Long waves and cyclone waves. *Tellus* **1** 33-52
Emanuel, K. A.	1989	The finite-amplitude nature of tropical cyclogenesis. *J. Atmos. Sci.*, **46,** 3431-3456
Emanuel, K. A.	1995	The behaviour of a simple hurricane model using a convective scheme based on subcloud-layer entropy equilibrium. *J. Atmos. Sci.*, **52,** 3960-3968
Hollingsworth, A.	1995	A spurious mode in the "Lorenz" arrangement of ϕ and T which does not exist in the "Charney-Philips" arrangement. *ECMWF Tech. Memo.* **211,** 12 pp.
Jordan, C. L.	1957	Mean soundings for the West Indies area. *J. Meteor.*, **15,** 91-97
Kurihara, Y., and R. E. Tuleya	1974	Structure of a tropical cyclone developed in a three-dimensional numerical simulation model. *J. Atmos. Sci.*, **31,** 893-919
Lorenz, E. N.,	1960	Energy and numerical weather prediction. *Tellus*, **12**, 364-373
Nguyen, C. M., R. K. Smith, H. Zhu, and W. Ulrich	2002	A minimal axisymmetric hurricane model. *Quart. J. Roy. Meteor. Soc.* **128** (in press)
Ooyama, K. V.	1969	Numerical simulation of the life cycle of tropical cyclones. *J. Atmos. Sci.*, **26,** 3-40
Rotunno, R., and K. A. Emanuel	1987	An air-sea interaction theory for tropical cyclones. Part II: Evolutionary study using a nonhydrostatic axisymmetric numerical model. *J. Atmos. Sci.*, **44**, 542-561
Smith, R. K.	2000	The role of cumulus convection in hurricanes and its representation in hurricane models. *Rev. Geophys.*, **38,** 465-489
Tokioka, T.	1978	Some consideration on vertical differencing. *J. Meteor. Soc. Japan*, **56**, 89-111
Weber, H. C., and R. K. Smith	1993	The stability of barotropic vortices: implications for tropical cyclone motion. *Geo. Astro. Fluid Dyn.*, **70**, 1-30
Zhu. H., R. K. Smith and W. Ulrich	2001	A minimal three-dimensional tropical cyclone model. *J. Atmos. Sci.*, **58** 1924-1944
Zhu. H., and R. K. Smith	2002	The importance of three physical processes in a minimal three-dimensional tropical cyclone model. *J. Atmos. Sci.*, **59**, 1825-1840

Appendix

8. Discrete Equations

Referring to the notation of Fig. 2, the discrete form of the continuity equation is

$$\frac{\partial p^*}{\partial t} + \nabla \cdot (p^* \mathbf{v})_l + \frac{1}{(\Delta\sigma)_l}[(p^*\dot{\sigma})_{l+1/2} - (p^*\dot{\sigma})_{l-1/2}] = 0 \quad (l = 1, 2, 3), \tag{A.1}$$

where $(\Delta\sigma)_l = \sigma_{l+1/2} - \sigma_{l-1/2}$ and the boundary conditions on $\dot{\sigma}$ are

$$(p^*\dot{\sigma})_{\frac{1}{2}} = (p^*\dot{\sigma})_{3\frac{1}{2}} = 0. \tag{A.2}$$

The discrete form of the thermodynamic energy equation is

$$\frac{\partial}{\partial t} p^* c_p T_{l+1/2} + \nabla \cdot [(p^*\mathbf{v})_{l+1/2} c_p T_{l+1/2}] + \frac{c_p}{(\delta\sigma)_{l+1/2}}[(Tp^*\dot{\sigma})_{l+1} - (Tp^*\dot{\sigma})_l] = (p^*\alpha\omega)_{l+1/2} + (p^* Q_\theta)_{l+1/2} \quad (l = 1, 2), \tag{A.3}$$

where

$$(p^*\mathbf{v})_{l+1/2} = \frac{1}{2(\delta\sigma)_{1+1/2}}[(\delta\sigma)_l (p^* v)_l + (\delta\sigma)_{l+1}(p^* v)_{l+1}] \tag{A.4}$$

and $(\delta\sigma)_{l+1/2} = 0.5[(\delta\sigma)_l + (\delta\sigma)_{l+1}]$.

In Eq. (A.3),

$$(Tp^*\sigma)_l = \frac{1}{2}[T_{l-1/2}(p^*\dot{\sigma})_{l+1/2} + T_{l+1/2}(p^*\dot{\sigma})_{l-1/2}] \quad (l = 1, 2, 3), \tag{A.5}$$

and

$$(p^*\alpha\omega)_{l+1/2} = \frac{RT_{l+1/2}}{p_{l+1/2}}[-p^* \times \sum_{k=1}^{l} \nabla \cdot (p^*\mathbf{v}_k)(\delta\sigma)_k + (p^*\mathbf{v})_{l+1/2} \cdot \nabla p_{l+1/2}] \quad (l = 1, 2). \tag{A.6}$$

At the upper and lower boundaries,

$$\frac{\partial}{\partial t}(p^* c_p T_{\frac{1}{2}}) + \nabla \cdot [(p^*\mathbf{v})_1 c_p T_{\frac{1}{2}}] + \frac{c_p T_{\frac{1}{2}}}{(\delta\sigma)_1}(p^*\dot{\sigma})_{\frac{3}{2}} = (p^* Q_\theta)_{\frac{1}{2}}. \tag{A.7}$$

and

$$\frac{\partial}{\partial t}(p^* c_p T_{3\frac{1}{2}}) + \nabla \cdot [(p^*\mathbf{v})_3 c_p T_{3\frac{1}{2}}] - \frac{c_p T_{3\frac{1}{2}}}{(\delta\sigma)_3}(p^*\dot{\sigma})_{2\frac{1}{2}} = (p^*\alpha\omega)_{3\frac{1}{2}} + (p^* Q_\theta)_{3\frac{1}{2}}, \tag{A.8}$$

In the previous equation,

$$(p^*\alpha\omega)_{3\frac{1}{2}} = \frac{RT_{3\frac{1}{2}}}{p_{3\frac{1}{2}}}[-p^* \sum_{k=1}^{3} \nabla \cdot (p^*\mathbf{v}_k)(\delta\sigma)_k + (p^*\mathbf{v})_3 \cdot \nabla p_{3\frac{1}{2}}]. \tag{A.9}$$

The moisture equation takes the discrete form

$$\frac{\partial}{\partial t} p^* q_{l+1/2} + \nabla \cdot [(p^*\mathbf{v})_{l+1/2} q_{l+1/2}] + \frac{1}{(\delta\sigma)_{l+1/2}}[(p^* q\dot{\sigma})_{l+1} - (p^* q\dot{\sigma})_l] = (p^* Q_q)_{l+1/2} \quad (l = 1, 2), \tag{A.10}$$

where $(p^*\mathbf{v})_{l\frac{1}{2}}$ and $(\delta\sigma)_{l+\frac{1}{2}}$ is the same as the thermodynamic energy equation and

$$(p^*q\dot{\sigma})_l = \frac{1}{2}[p^*q_{l-\frac{1}{2}}\dot{\sigma}_{l-\frac{1}{2}} + p^*q_{l+\frac{1}{2}}\dot{\sigma}_{l+\frac{1}{2}}], \tag{A.11}$$

where the value of q and $\dot{\sigma}$ at the half levels are simply interpolated by an arithmetic average.

At the upper and lower boundaries,

$$\frac{\partial}{\partial t}(p^*q_{\frac{1}{2}}) + \nabla\cdot[(p^*\mathbf{v})_1 q_{\frac{1}{2}}] + \frac{q_{\frac{1}{2}}}{(\delta\sigma)_1}(p^*\dot{\sigma})_{\frac{3}{2}} = (p^*Q_q)_{\frac{1}{2}}, \tag{A.12}$$

and

$$\frac{\partial}{\partial t}(p^*q_{3\frac{1}{2}}) + \nabla\cdot[(p^*\mathbf{v})_3 q_{3\frac{1}{2}}] - \frac{q_{3\frac{1}{2}}}{(\delta\sigma)_3}(p^*\dot{\sigma})_{2\frac{1}{2}} = (p^*Q_q)_{3\frac{1}{2}}. \tag{A.13}$$

The discrete form of the hydrostatic equation is

$$\Phi_l - \Phi_{l+1} = \frac{(p_{l+\frac{3}{2}} - p_{l-\frac{1}{2}})RT_{l+\frac{1}{2}}}{2p_{l+\frac{1}{2}}} \quad (l = 1, 2). \tag{A.14}$$

At the lower boundary,

$$\Phi_3 - \Phi_{3\frac{1}{2}} = \frac{(p_{3\frac{1}{2}} - p_{2\frac{1}{2}})RT_{3\frac{1}{2}}}{2p_{3\frac{1}{2}}} \tag{A.15}$$

The equation for the vertical $\sigma-$ velocity takes the discrete form

$$\dot{\sigma} = -\frac{1}{p^*}\sum_{k=1}^{l}\nabla\cdot(p^*\mathbf{v})_k(\delta\sigma)_k + \frac{\sigma}{p^*}\sum_{k=1}^{3}\nabla\cdot(p^*\mathbf{v})_k(\delta\sigma)_k \quad (l = 1, 2). \tag{A.16}$$

At the upper and lower boundaries, $(p^*\dot{\sigma})_{\frac{1}{2}} = (p^*\dot{\sigma})_{3\frac{1}{2}} = 0$.

The horizontal pressure gradient force is simply calculated by,

$$-(\nabla_p\Phi)_l = -(\nabla_\sigma\Phi)_l - (\frac{RT\sigma}{p}\nabla p^*)_l \quad (l = 1, 2, 3), \tag{A.17}$$

a formulation in which mass conservation is satisfied also.